

# Glyph-Based Video Visualization for Semen Analysis

Brian Duffy, *Member, IEEE*, Jeyan Thiyagalingam, Simon Walton, David J. Smith, Anne Trefethen, Jackson C. Kirkman-Brown, Eamonn A. Gaffney and Min Chen, *Member, IEEE*

**Abstract**—The existing efforts in computer assisted semen analysis have been focused on high speed imaging and automated image analysis of sperm motility. This results in a large amount of data, and it is extremely challenging for both clinical scientists and researchers to interpret, compare and correlate the multidimensional and time-varying measurements captured from video data. In this work, we use glyphs to encode a collection of numerical measurements taken at a regular interval and to summarize spatio-temporal motion characteristics using static visual representations. The design of the glyphs addresses the needs for (a) encoding some 20 variables using separable visual channels, (b) supporting scientific observation of the interrelationships between different measurements and comparison between different cells and their flagella, and (c) facilitating the learning of the encoding scheme by making use of appropriate visual abstractions and metaphors. As a case study, we focus this work on video visualization for computer-aided semen analysis, which has a broad impact on both biological sciences and medical healthcare. We demonstrate that glyph-based visualization can significantly increase insight into cell function by revealing changes that are not obvious through current analysis techniques.

**Index Terms**—Video visualization, glyph visualization, motion summarization, multivariate data, semen analysis, flagellum locomotion

## 1 INTRODUCTION

Over the past decade, researchers have demonstrated the usefulness of video visualization through applications such as surveillance [23], [16], sports analysis [58] and entertainment [24], [49]. In biology today, videos are used extensively to capture motile cells, many of which exhibit a tail-like appendage called a *flagellum*. Video data is used by biomathematicians across applied mathematics fields to reverse engineer the mechanics of naturally occurring phenomena such as a cell's flagellum. The most commonly encountered flagella are in the sperm cells of mammals. The motion of a swimming sperm is difficult to characterize using elementary measurements such as velocity, because it varies in time, and rarely follows a straight line. Motility is caused by the complex movement of the flagellum which cannot be characterised by a single numerical value. As shown in Fig. 1, the existing visual representations for such a motion typically depict only the motion path of the cell head, or a sequence of geometries of the flagellum. While Fig. 1(a) conveys a limited amount of information, it is non-trivial to discern meaningful motion characteristics from those in Fig. 1(b,c). One challenge is to devise an effective visual representation that can summarize

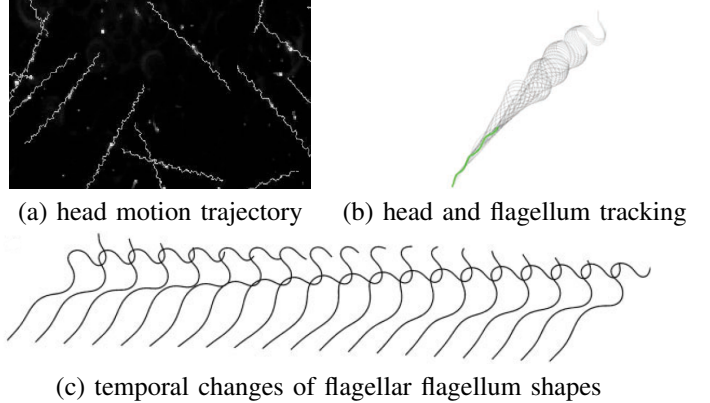


Fig. 1: Existing visualization of sperm convey a limited amount of information about motion characteristics. Images are from [61].

the motion of many hundreds of cells in a video, while depicting a collection of measurable motion characteristics.

Computer-Assisted Semen Analysis (CASA) is a collection of techniques for providing quantitative measurements of a semen sample captured using a camera or a digitizing tablet through a microscope [47], [2], [14], [68], [27], [48]. Typical measurements include sperm count and up to nine different motility parameters. In recent years, scientists have proposed a number of new motility parameters in addition to the nine CASA parameters. This work is partly motivated by the need to find better prognostic measurements than currently exist and partly by the challenge of summarizing flagellum motion which has not been tackled in any previous work on video visualization.

In order to address the need for depicting a large set of

• B. Duffy is with the Oxford Centre for Collaborative Applied Mathematics (OCCAM), University of Oxford  
 • J. Thiyagalingam, S. Walton, A. Trefethen and M. Chen are with the Oxford eResearch Center (OeRC), University of Oxford  
 • D. J. Smith is with the School of Mathematics, University of Birmingham  
 • E. A. Gaffney is with the Centre for Mathematical Biology (CMB), University of Oxford  
 • J. C. Kirkman-Brown is with The Centre for Human Reproductive Science at the Birmingham Women's Hospital and the School of Clinical and Experimental Medicine, University of Birmingham

parameters while maintaining spatiotemporal context associated with individual sperm, we propose the use of purposely-designed glyphs to encode the multivariate data space. This approach allows biomathematicians to compare the interrelationships between some 20 motility measurements. Most existing work on glyph-based visualization typically deals with 3-5 attribute dimensions, with perhaps the highest dimensionality in glyph-based visualization for DTI datasets [15], [38]. It is therefore not a trivial design problem to encode a data space with some 20 dimensions. Furthermore, it is necessary for the visual representation to facilitate effective learning, memorizing and using the encoding scheme by domain specialists. We also recognize the advantageous fact that scientists are more capable of handling a slightly more complex glyph encoding scheme with appropriate visual abstractions and metaphors. Our summarization scheme and glyph designs reveal changes in cell motility that are not obvious from watching videos or analysing single parameters.

Our contributions are as follows:

- We have developed a novel visualization method for the summarization and depiction of sperm and flagellum motion captured on videos;
- We have stretched the capability of glyph-based visualization to encode a high-dimensional data space with some 17 explicit parameters, while making use of appropriate visual abstractions and metaphors to address the needs for facilitating the learning of the encoding scheme;
- We have provided domain specialists with a tool for making observations of interrelationships between different measurements and effective visual comparisons between different flagella in the parameter space.

The remainder of this paper is organized as follows. In Section 2, we give a brief overview of current state-of-the-art in video and glyph-based visualization. In Section 3 we provide the application background of this work. In Section 4 we describe the data space that encapsulates the standard CASA measurements and additional measurements proposed by biomathematicians. In addition, we outline the process for obtaining various measurements from videos and discuss the need to consider uncertainty in visualization. In Section 6, we describe the design principles followed by this work and the process of attaining the effective glyph design for this application. In Section 7, we present and discuss the results of visualization, together with a brief description of our implementation. We report the evaluation by domain specialists in Section 9, offer our concluding remarks in Section 10.

## 2 RELATED WORK

The goal of this work is to incorporate multivariate, spatial and uncertainty visualization techniques into a unified system for biomathematicians. Techniques from video (Section 2.1) and glyph-based visualization (Section 2.2) are used.

### 2.1 Video Visualization

Video visualization is a collection of graphics and visualization techniques concerned with the creation of a new visual

representation from an input video to reveal important features and events in the video. Meaningful information is extracted from videos and conveyed to users in summary or abstract representations. Video visualization assists users in intelligent reasoning by summarizing video content, removing the burden of viewing videos. This aim justifies deflection from creation of realistic imagery and instead advocates simplifications, abstraction and embellishments if they improve understanding.

*Image-based techniques* segment videos into frames, shots and scenes [50]. Detection of keyframes in these applications is crucial [63]. There are three different approaches to shortening the time of watching videos: video navigation techniques [44], [53], [59], [17], video montage and video synopsis [34] and video skimming techniques [63], [10].

*Abstract techniques* summarize attributes of a video, such as changes in a scene, changes between frames, motion flow and pixel clusters, depicting these attributes visually to aid understanding of video using a small number of visualizations [13], [9]. Such visualizations may not display objects directly but the abstract representation can convey temporal attributes more effectively than discrete keyframe displays.

The development of the subject has been heavily influenced by many applications in entertainment [24], [49], sports [58], [29], [43], security [7] and taxonomy visualization [46]. A recent survey by Borgo *et al.* [6] proposed a new taxonomy to categorize the concepts and techniques in this newly-emerged body of knowledge. In addition Borgo *et al.* [6] give a concise overview of the major advances in automated video analysis.

### 2.2 Glyph-based Visualization

Glyph visualization is a form of visual design where data is depicted by a collection of visual objects. Its major strength is that patterns of multivariate data can be more readily perceived in a spatial context. Glyph design is related to semiology [4], the theory of signs and symbols in the communication of information. Glyphs are composed of basic components, each with expressive power and can utilize various visual channels such as visualization, size, shape, orientation, texture, and symbol.

Glyphs are utilized in medical applications to provide pre-attentive visualizations to raw imagery [56], [55]. They can also be placed interactively where an initial dense glyph packings can be modified via mouse interaction [28]. Wong *et al.* [67] present a glyph layering strategy for visualization of multivariate climate data. In vector field visualization, glyphs are discussed and compared with other forms of visualization in a collection of surveys on flow visualization [52], [41]. Kirby *et al.* [39] utilize concepts from oil painting in order to visualise multivariate data from incompressible fluid flow simulations. Ropinski *et al.* [57] integrate glyphs into the volume rendering pipeline, overlaying glyphs on isosurfaces of volume data. Crawfis *et al.* [11] define a language for combining data of different frequencies (images, vectors, glyphs, surfaces, etc) using primitive operators.

Ward [65] gives a taxonomy for glyph placement strategies in multidimensional data visualization. Fuchs *et al.* [19] provide a thorough overview of glyph-based visualization for

the scientific community. A survey by Ward [64] provides a technical framework for glyph-based visualization, covering aspects of visual mapping and layout, as well as important issues such as bias in mapping and interpretation.

### 3 APPLICATION BACKGROUND

Since the early application of image analysis to semen samples (e.g., [3]), Computer Aided Semen Analysis (CASA) has become a mature technology, which is now commercially delivered to hospitals and fertility clinics by several manufacturers. The technology enables the quantitative measurement of sperm motility and kinematics, with the more recent ability to estimate sperm concentration and semi-automated morphology analysis. CASA has three distinct advantages over manual methods. Firstly, it provides more objective, and potentially more accurate methods for analyzing semen samples. Secondly, it provides quantitative measurements of the kinematic parameters of cells (forward progression, hyperactivated motility, characteristics of capacitated cells) that surpass manual methods of computation in speed and accuracy. Finally, it provides morphology measurements of dead sperm, which is beyond the scope of this paper.

However, with any developing technology there are issues. CASA accuracy in tracking and classifying cells can be compromised by contaminants of semen such as white blood cells. Digital motility measurements may be more accurate when appropriate steps are taken to prepare samples, which is the approach taken in this paper. The technology is still improving, and the automatic computer vision techniques for tracking and classifying cells remain the bottleneck. The WHO [68] currently endorses manual counting as the “gold standard” for an accurate sperm count with the disadvantage that no quantitative motility data can be recorded. Manual methods are still used extensively due to accuracy, flexibility and unavailability of costly equipment.

Furthermore, the current technology only conveys global statistics of the video data to the users through a small set of numerical values. It is difficult for users to gain insight into the characteristics of individual cells that contribute to the overall multivariate statistics, or to verify the accuracy and appreciate the uncertainty in the automated process. This is one of the motivations of this work.

The guidelines for the preparation and analysis of human semen are outlined by the World Health Organization (WHO) [68]. Measures of sperm motion for automatic analysis of videomicrography were first established in a report by Jecht and Russo [32] and subsequently numerous authors such as, Katz, Holt and Hobson have developed the field as outline in [2]. Katz and Davis [36], [35] presented algorithms for computing motility measures of sperm based on the path shape and instantaneous turning angles. Subsequently these measures have become the standard for sperm motility analysis, outlined by the WHO laboratory manual [68], as shown in Fig. 2.

Additionally, researchers in experimental reproductive sciences capture mechanical data of flagella from videos of sperm cells. Analysis of flagellum mechanics help researchers to characterise the biomechanical properties and energy requirements of different types of motility and properties of

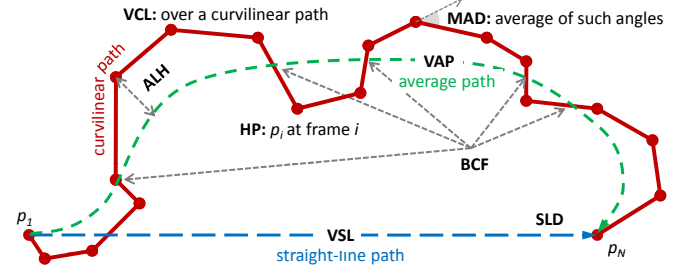


Fig. 2: The WHO laboratory manual [68] defines nine parameters for computer-aided semen analysis that relate to the kinematics of the swimming cell. The cell is treated as a particle as it is tracked in each frame. Here we show five of the nine parameters and their geometric interpretations.

potentially-fertilising sperm. This additional information offers the potential for increased insight into sperm motility in the context of assessing environmental risk factors [37] and pre-clinical reproductive toxicology [33]. Detailed flagellar information also enables novel explorations of flagellar mechanics and enables interrogation of hypotheses for the molecular motor regulation controlling cellular swimming [20].

### 4 MEASUREMENTS IN SEMEN ANALYSIS

In biology research, sperm kinematic and mechanical measures are used to characterize sperm swimming patterns. The kinematic measures used in Section 4.1 are those discussed in the WHO manual [68] and are defined by Katz and Davis [35]. However we note here that algorithms for measuring sperm kinematics vary widely as discussed in [68]. For an in-depth discussion of the evolution of the current state-of-the-art in sperm kinematics we refer readers to Mortimer [47]. Section 4.2 defines formulae for measuring morphology and mechanics measures of the cell head. Finally, Section 4.3 defines the mechanical measures of the flagellum. In this paper, we ignore rare aberrant morphological cases, such as cells with irregular and odd shapes or with multiple heads and flagella.

#### 4.1 Kinematic Measures of the Head

CASA systems track the centroid of the head of each cell, typically for a period of 1 second, the standard tracking time defined in [68]. The resulting set of centroids is used to analyze the kinematics of the cells. The path the sperm takes through the video is referred to as a track and is represented by a list of head positions (**HP**),  $p_i$ , of the cell for each frame  $i$ . Using this, the following kinematic measure of velocity, swimming pattern and progressiveness are computed as in Fig. 2.

**VCL, Curvilinear Velocity ( $\mu\text{m}/\text{s}$ )** : The time-averaged velocity of a sperm along its actual curvilinear path, over  $N$  frames, as perceived in the microscope. The instantaneous velocity  $v_{ci}$  of the sperm is computed using three consecutive points on the path,  $p_{i-1}$ ,  $p_i$  and  $p_{i+1}$  with a regular time interval  $\Delta t$ . The velocity  $v_{ci}$  is computed for each frame  $i$  as:

$$v_{ci} = \frac{\|p_i - p_{i-1}\| + \|p_{i+1} - p_i\|}{2\Delta t}.$$

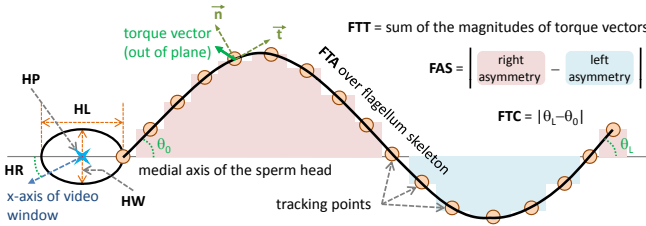


Fig. 3: Sperm measures are computed by fitting geometry to cells extracted from video data. Head morphology (**HP**, **HL**, **HW**, **HR**) and flagellum mechanics (**FTA**, **FTC**, **FTT**, **FAS**) are approximated using integration from this proxy geometry.

VCL is computed by summing the instantaneous velocities for each frame and computing the time-average as follows:

$$VCL = \frac{1}{N\Delta t} \sum_{i=1}^N vc_i. \quad (1)$$

where  $N$  is the number of frames in a standard 1 second period.

**VSL, Straight-Line (Rectilinear) Velocity ( $\mu m/s$ )**: The time-averaged velocity of a sperm along the straight line between the end points of its curvilinear path over a standard 1 second period.

**VAP, Average Path Velocity ( $\mu m/s$ )**: The time-averaged velocity of a sperm along its average path. The instantaneous average velocities  $va_i$  are computed from the smoothed average path given by the set of points  $\bar{p}_i = (\bar{x}_i, \bar{y}_i)$  and is computed in the same way as  $vc_i$ . In addition to velocity, angular measures are useful in discriminating between sperm exhibiting widely different swimming patterns [35].

**ALH, Amplitude of Lateral Head Displacement ( $\mu m$ )**: Magnitude of lateral displacement of a sperm head about its average path. It can be expressed as a maximum or an average of such displacements. Different CASA instruments compute ALH using different algorithms, so values may not be comparable among systems.

**BCF, Beat-Cross Frequency (Hz)**: The average rate at which the curvilinear path crosses the average path.

**MAD, Mean Angular Displacement (degrees)**: The time-averaged absolute values of the instantaneous turning angle, denoted by  $\theta_i$ , of the sperm head along its curvilinear path.

In addition, a number of abstract measures of the progressiveness of the sperm swimming may also be computed. The straight line direction **SLD**. The linearity of a curvilinear path is the ratio  $LIN = VSL/VCL$ . The measure of oscillation of the curvilinear path about the average path, or wobble, is the ratio  $WOB = VAP/VCL$ . Finally, linearity of the average path is given by the ratio  $STR = VSL/VAP$ .

## 4.2 Head Rotation Analysis

The rotation of the sperm cell between frames can be detected by changes in the observed shape of the cell head since it is projected onto the microscope focal plane. A number of pixels are extracted that represent the head of the cell in each frame. The length **HL** and width **HW** of the head, measured in  $\mu m$ , of the sperm cell are estimated by ellipse fitting [21]. This allows us to determine subtle changes in the head's shape and rotation **HR** in degrees, such as whether the cell is planar

swimming. In general, this is sufficient for human sperm as the head is convex. The centroid of the head is used to track the sperm's location, i.e., the **HP** measure mentioned at the beginning of Section 4.1.

## 4.3 Flagellum Mechanics Analysis

Each tail-like flagellum is represented by a polyline and is tracked through the video. Each polyline at time  $k$  is stored as a series of points  $q_{k,1}, q_{k,2}, \dots$ . As the flagellum is almost featureless in the image, it is not possible to determine each point precisely in different frames. When we assume that a sperm is swimming more or less in a 2D space under the microscope, the arclength of the flagellum is a more reliable factor than any feature-based tracking of points on the flagellum. We hence sample each polyline equally to obtain a point set with  $L$  points.

**FTA, Total Projected Arclength ( $\mu m$ )**: The total arclength of a flagellum at time  $t$ ,  $FTA_k$ , is computed as the sum of the Euclidean distances between the consecutive points:

$$FTA_k = \sum_{j=1}^{L-1} \|q_{k,j+1} - q_{k,j}\| \quad (2)$$

**FTC, Change in Angle (degrees)**: The difference between the angle of the flagellum at the head  $\theta_{k,1}$  and the angle of the flagellum at the tip  $\theta_{k,L}$ . This gives the total amount of sliding undertaken by the flagellum about its centreline as in Fig. 3.

**FTT, Total Torque  $N\mu$** : The viscous torque per unit length represents the tendency of the flagellum to induce rotational motion. Assuming planar beating, the torque is implicitly in the direction out of the beat plane, as shown in Fig. 3. From resistive force theory [25], [45], the viscous drag force per unit length,  $F$ , exerted by the flagellum on the fluid is:

$$F = C_T(\vec{t} \cdot \vec{u})\vec{t} + C_N(\vec{n} \cdot \vec{u})\vec{n} \quad (3)$$

where  $C_T$  and  $C_N$  are resistance coefficients. Using the definition by Gray and Hancock [25],  $\vec{t}$  is the tangent vector,  $\vec{n}$  is normal to  $\vec{t}$  in the plane and  $\vec{u}_{k,j}$  is the rate of change of the flagellum over the video frames  $i$ . This computation yields a vector whose components describe the viscous drag in the  $x$  and  $y$  directions. From Equation 3 we can derive the total torque over the flagellum, where  $F_{k,j}^x = (C_T(\vec{t} \cdot \vec{u})\vec{t}_x)_{k,j}$  and  $G_{k,j}^x = (C_N(\vec{n} \cdot \vec{u})\vec{n}_x)_{k,j}$  in the  $x$  direction and similarly in the  $y$  direction. The viscous torque per unit length is  $FTT_{(k,j)} = \vec{q}_{k,j} \times \vec{f}_{k,j}$  and  $\vec{f}_{k,j} = [F_{k,j}^x + G_{k,j}^x, F_{k,j}^y + G_{k,j}^y]$ . Therefore the total viscous torque the flagellum exerts on the fluid at  $FTT_k$  is the discrete sum of the magnitudes of the vector components:

$$FTT_k = \left| \sum_{j=1}^{L-1} (\vec{q}_{k,j}^x \vec{f}_{k,j}^y - \vec{q}_{k,j}^y \vec{f}_{k,j}^x) \delta s \right| \quad (4)$$

We use only  $FTT_k$  as its sign correlates with the asymmetry.

**FAS, Asymmetry**: The asymmetry of the flagellum about the medial axis of the head is a standard indicator of hyperactivated swimming, which is functionally critical for successful fertilization and is required to penetrate the oocyte. As illustrated in Fig. 3, asymmetry is measured by integrating the amplitudes of the flagellum about the medial axis of the head.

TABLE 1: A total of 20 measures discussed in Section 4 and their corresponding computational characteristics.

measure	type	semantics	frame	interval
<b>HP</b>	$\mathbb{R}^2$	position	yes	—
<b>SLD</b>	$\mathbb{R}^2$	direction	yes	average
<b>VCL</b>	$\mathbb{R}$	velocity	—	yes
<b>VSL</b>	$\mathbb{R}$	velocity	—	yes
<b>VAP</b>	$\mathbb{R}$	velocity	—	yes
<b>ALH</b>	$\mathbb{R}$	distance	yes	average
<b>BCF</b>	$\mathbb{R}$	counting	—	yes
<b>MAD</b>	$\mathbb{R}$	angle	yes	average
<b>LIN</b>	$\mathbb{R}$	ratio	—	yes
<b>WOB</b>	$\mathbb{R}$	ratio	—	yes
<b>STR</b>	$\mathbb{R}$	ratio	—	yes
<b>HL</b>	$\mathbb{R}$	length	yes	average
<b>HW</b>	$\mathbb{R}$	width	yes	average
<b>HR</b>	$\mathbb{R}$	angle	yes	average
<b>FTA</b>	$\mathbb{R}$	length	yes	average
<b>FTC</b>	$\mathbb{R}$	angle	yes	average
<b>FTT</b>	$\mathbb{R}$	torque	yes	average
<b>FAS</b>	$\mathbb{R}$	balance	yes	average
<b>UH</b>	[0, 1]	uncertainty	yes	average
<b>UF</b>	[0, 1]	uncertainty	yes	average

#### 4.4 Uncertainty in Sperm Cell Extraction

The video data considered in this work was captured using phase contrast microscopy. The video processing algorithms had to deal with a number of technical challenges in object recognition, segmentation and tracking because of background noise, debris, and close proximity of flagella in each frame. It is thus necessary to convey the potential errors in video processing to the users. We thus introduced uncertainty measures at every stage of the video processing pipeline. Image processing techniques such as segmentation and morphological operations facilitate target tracking of sperm heads. We estimate an uncertainty measure (**UH**) for all processing related to a sperm head, and another measure (**UF**) for all processing related to a sperm flagellum. The measurements are computed based on the following factors:

- the distinction of an object (head or flagellum) from detractors (noise, debris) is uncertain (close to the threshold);
- the tracking algorithm fails to recognize an expected and previously recognized object;
- the tracking algorithm is confused by multiple, similarly-moving objects;
- the segmentation of an object yields a significantly different set of measures (e.g., flagellum length, pixel occupancy) in comparison with an expected object or previously tracked and segmented object;

These two uncertainty measures, **UH** and **UF**, are visualized in conjunction with the other measures discussed in the previous subsections.

## 5 BRUTE FORCE VISUALIZATION

In Sections 4.1 - 4.4, we described a total of 20 measures, some of which can be obtained at individual frames, and some can be computed over a temporal interval. They are all represented by real numbers but vary in their basic semantic meaning. Table 1 summarizes some computational characteristics of these measures.

Naïvely, each measure can be visualized as a time series plot, which also applies to those measures computed over a regular interval. Hence in brute force, one can visualize the motion characteristics of each sperm using one scatter plot for **HP** and **SLD** and some 18 time series plots for the others. To compare  $N$  cells, one can juxtapose  $N$  sets of measures in each of the 19 plots. It is not difficult to imagine that such visual representations will not be effective for the domain experts to make meaningful observation. Not only is there a huge cognitive load in visual search for individual measures and in assembling a mental picture for the motion characteristics of each sperm, but also an absence of spatial context in viewing the time series plots.

One alternative visual representation is parallel coordinate visualization, which may have 20 real axes for the 19 interval-based measures with a total of  $\mathbb{R}^{20}$  dimensionality. The measure of each sperm can be displayed as a line across different axes. For multiple time intervals,  $T_1, T_2, \dots$ , one can make use of additional parallel coordinate visualizations, each encode measures in a specific time interval  $T_i$ . It is not difficult to observe the shortcoming of such visual representations. There is a complete absence of spatial context, while it is a cognitive burden in searching for different measures. Users will also be required to try different ordering of axes in order to make observation about the correlation between various measures. Furthermore, when using multiple parallel coordinates to depict measures in a series of time intervals, it would be very difficult to observe temporal behavioral changes of individual cells.

## 6 GLYPH-BASED VISUAL DESIGN

In order to bridge the gap between statistical measurements and intuitive scenario observation, we adopted glyph-based visualization. We divide video frames into a series of temporally-ordered subsets of a pre-defined *reference period*,  $T_{ref}$ , which corresponds to the standard duration of measurement,  $T_{ref} = 1sec$ , as defined in the WHO manual [68]. Hence, the motion characteristics of each sperm can be computed in regular intervals defined by  $T_{ref}$ , and the statistical measurements in each interval can be mapped to a glyph. For a sperm captured in a video, the series of temporal subsets of frames enables the sperm to be depicted as a series of glyphs as in Fig. 9. The domain experts had the following requirements.

- 1) The primary requirement is the need to encode some 20 measurements in a single glyph. This presents a huge challenge as all measurements are numerical rather than categorical, while the existing works in the literature have so far attempted up to 12 attribute dimensions.
- 2) Because the main objective of this work is to enable scientists to make observations about the interrelationship between different measurements, it will not be appropriate to make a priori assumptions about the importance of these measurements. The absence of an importance order results in the lack of definite guidelines about selecting visual channels according to the order of their discriminative capacities.

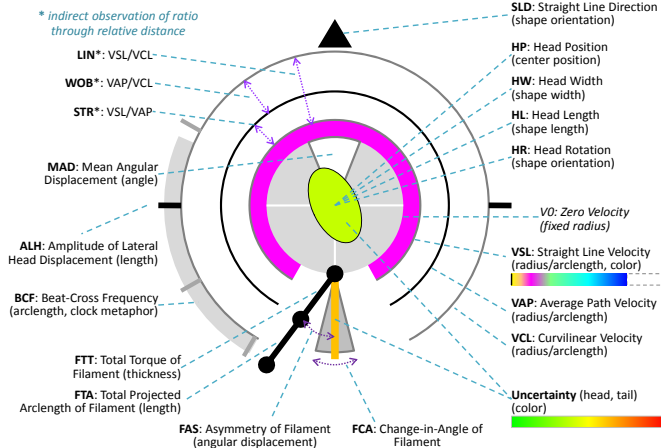


Fig. 4: Glyph Schematic: this schematic shows how 17 parameters are explicitly encoded into the the glyph. Parameters such as LIN, WOB and STR are implicitly represented by how the velocity parameters are laid out in the glyph.

- 3) Some measurements are related (e.g., VSL, VCL, VAP, ALH, etc.) and there is a need to support comparative analysis for different measurements within the context of a single sperm.
- 4) It is desirable for the visual design to enable the depiction of the visual signatures of some major classes of cells, such as live *vs.* dead, human sperm cells *vs.* mouse sperm cells.
- 5) It is necessary for the visual design to facilitate effective perception and cognition. Although it is not a requirement to be able to judge numerical values accurately (as glyphs will not be the best tool for such tasks), it would be helpful that each attribute identified can be individually compared across many glyphs spatially and temporally.
- 6) Some domain specialists expressed a wish to have a glyph resembling a sperm, which poses an interesting challenge. While it indicates the importance for the visual representation to exhibit some metaphoric design features, it is a non-trivial requirement as the realistic representation of a sperm, especially its bendy flagellum, was a causal factor for the difficulties to observe motion characteristics.

We made use of the glyph design principles and the relevant literature in [46]. Here we only discuss the most relevant ones to avoid repetition. In perception, there is a rich collection of studies on *integral* and *separable* dimensions of visual channels. In general, given two visual channels with dissimilarity of  $d_a$  and  $d_b$ , the combined dissimilarity of an integrated design is about their Euclidean distance  $\sqrt{d_a^2 + d_b^2}$  [40], [26]. On the other hand, the combined dissimilarity of separable visual channels is close to their city-block distance  $d_a + d_b$  [8], [60]. We adopt the latter concept as the most important design principle in this work. To enable different attribute dimensions to be mapped onto separable visual channels, we first try to encode different dimensions using spatially independent lines or shapes. Secondly, in some cases where we have to use the same line or shape to encode more than one attribute in order

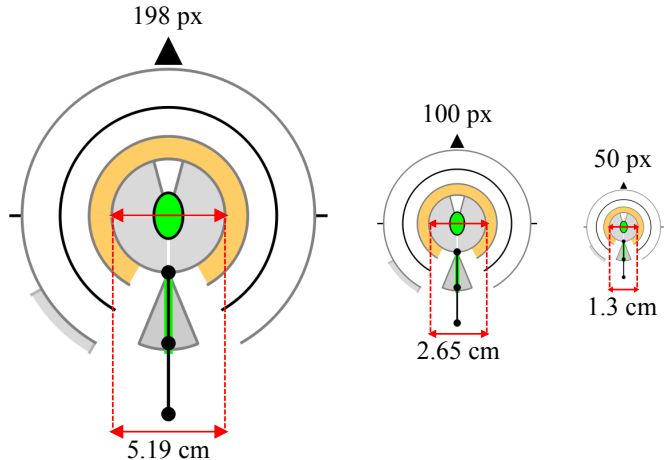


Fig. 5: The scale at which the glyph becomes illegible. Each glyph is annotated with the approximate width in pixels and centimeters of the diameter of the zero velocity ring as described in Fig. 4. The zero velocity ring is a constant size in every glyph displayed at a specific scale.

to reduce clutter, we ensure that the host shape will never disappear because one attribute value is too small. Thirdly, we do not use different color dimensions (e.g., RGB or HSV) to encode different attributes. We avoid using opacity in our encoding, though it can be safely deployed in many cases.

We started our design activities with a series of brainstorm meetings. We produced swatch charts for the major designs, and evaluated their suitability by considering issues such as visual channel separation, channel conflicts, scalability, compactness, clarity, attention bias, comparability, and metaphoric abstraction. An example of a swatch chart can be seen in Fig. 6. Fig. 5 shows the our glyph design at different scales. Here we can see the lowest resolution that the glyph is still legible.

We presented these designs to the domain specialists involved and sought their opinions. We found that the domain specialists responded better to more abstract glyph designs that made use of simple lines and shapes. After numerous iterations, occasionally involving debates and ranking exercises, we eventually converged into a design as illustrated in Fig. 4.

The design encodes a total of 20 attribute dimensions directly. These include 6 CASA parameters (VCL, VAP, VSL, BCF, ALH, MAD), 4 head measurements (HP, HW, HL, HR), 4 flagellum measurement (FTA, TCA, FAS, FTT), the straight line motion direction (SLD), and two uncertainty measurements in processing the head and flagellum data. In addition, 3 other CASA parameters (LIN, WOB, STR) can be observed indirectly by comparing VCL, VAP and VSL.

As this is a new approach that has not been previously experienced by the domain experts, we worked closely with biomathematicians and experts in semen analysis throughout the glyph design process. There were a number of challenges and sometimes conflicting requirements, which we list below.

The three velocity measurements, i.e., curvilinear (VCL), average path (VAP) and straight line (VSL), are the most used attributes in semen analysis. The visual comparison of these measurements is also important to observe three ratio factors,  $LIN = \frac{VSL}{VCL}$ ,  $WOB = \frac{VAP}{VCL}$  and  $STR = \frac{VSL}{VAP}$ . Although a color channel may facilitate a higher level attention, it

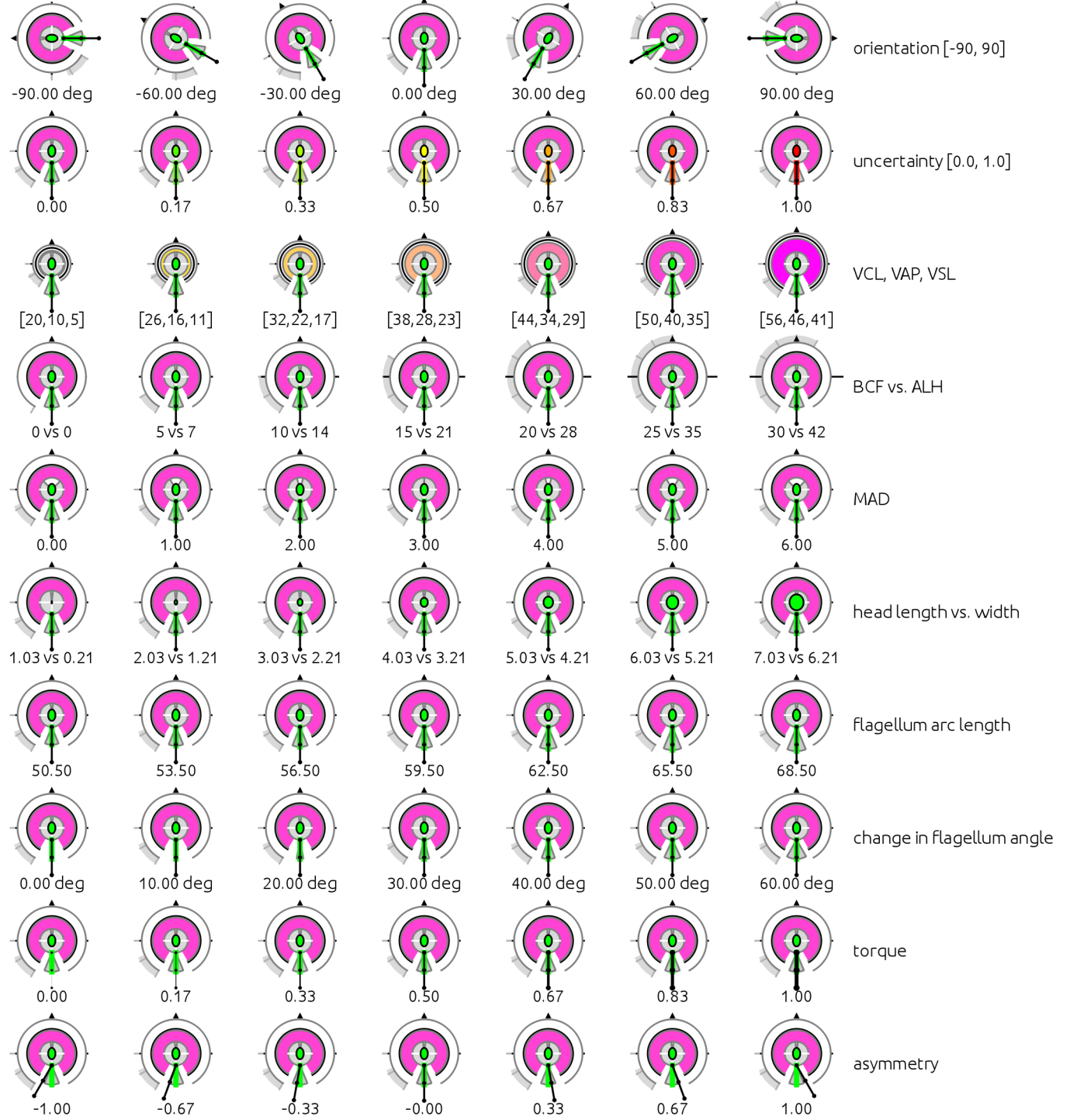


Fig. 6: The swatch chart shows how the parameters vary in the glyph so that researchers may become familiar with the possible configurations of the large number of parameters.

cannot encode many values while maintaining its discriminative capacity. We thus map these three attributes to the radii of three open ended arcs. This avoids the arcs being interpreted and compared as areas. As radii are linearly related to the circumferences, the line lengths offer equivalent but more scalable visual quantities. Metaphorically, velocity is associated with distance or length; hence these three mappings are easy to remember. Although we always have the spatial relationships  $VCL \geq VAP \geq VSL$ , we further improve their

identification by assigning a much darker color to the middle line, VAP. The geometrical mapping of these three velocities is defined as:

$$r_{vcl} = \frac{VCL + C_{base}}{C_{scale}}, \quad r_{vap} = \frac{VAP + C_{base}}{C_{scale}}, \quad r_{vsl} = \frac{VSL + C_{base}}{C_{scale}}$$

where  $C_{base}$  and  $C_{scale}$  are two user-definable constants.  $C_{scale}$  specifies the overall scaling factor of the glyph in relation to microns  $\mu m$ , the standard distance unit in semen analysis.

For example, if  $100 \mu\text{m}$  is mapped to 50 pixels,  $C_{scale}$  is set to 2.  $C_{base}$  specifies the minimal glyph radius to prevent the generation of glyphs that are too small to see. Since the velocity of a sperm affects the overall glyph size, a sperm that is not in motion could potentially be mapped to a tiny dot in the visualization. One normally sets  $C_{base}$  in relation to the maximum head length of the sperm to be studied. For glyphs in this paper, we set  $C_{base} = 80\mu\text{m}$  and  $C_{scale} = 5$ .

Normally, the ratio between VSL and VCL (i.e., LIN) varies between 0.2 and 0.8. However, sometimes it may become very small, at the scale of 0.01. Visually it will be difficult to distinguish between the VSL of such a sperm and the VSL of a dead one (note: there is little risk in mistaking a live one for a dead one as VCL and VAP would be large enough). To make VSL more perceptible, we add a redundant color channel for the circular strip between VSL and V0. This is one of three colored regions in the glyph; hence it is fairly noticeable. The colormap for VSL is shown in Fig. 7, which consists of six bands. While overcoming the visibility problem of VSL, also addresses requirement 4). Since the arc channel for VSL is not associate [4], colormap was also designed to facilitate metaphoric color symbolism (e.g., pink pig, grass-eating ram and sperm whale) to aid memorization. The positive effect of visual metaphors upon memory was confirmed in [5].

CASA attribute BCF (beat-cross frequency) created some difficulties for us as it encapsulates the number of interactions between VCL and VAP. We did consider several design options of using dots or short lines to represent BCF. However, because BCF varies between 2 and 35, it will be highly inefficient to rely on object counting as a visual mapping [66]. We thus mapped BCF to a shaded circular strip between VCL and VAP as shown in Fig. 4. It makes use of a common partition of a circumference into 60 sections. BCF can easily be estimated as one would estimate minutes on an analogue clock, starting from the 7 o'clock position, it is not difficult to identify key values of 0, 15 and 30 in relation to ALH and SLD.

A new measurement, FTT (total torque of flagellum) was another attribute that brought about many contentious design options. After many iterations, we decided to map it to the thickness of the pendulum line that was originally designed for representing FAS (flagellum asymmetry). Our initial instinct was to avoid loading two attributes onto the same object. However, after careful analysis we realized that the two visual channels can still be considered separable as the perception of thickness does not dependent on the angle of FAS (assuming effective anti-aliasing in rendering) and vice versa. It is necessary to ensure that the pendulum line will never disappear [22]. We achieve this by (a) setting its minimal thickness to 1 pixel, (b) setting its length as same as the radius for VCL, (c) always displaying the black pendulum head even if VCL = 0, and (d) assigning the highest display priority so it will not be occluded by other components of the glyph.

In addition, we made a number of metaphoric associations to help domain specialists remember the coding scheme, such as “beak” as a directional pointer (SLD), “big mouth” for “madness” (MAD or mean angular displacement), “pendulum” for imbalance (i.e., asymmetry or FAS), and “tail” for two of the major attributes of flagellum.

## 7 APPLICATION SCENARIOS

Scientists in semen analysis routinely deal with multivariate data when analyzing cells. They use this data to assess cell fitness and function. Glyph-based video visualization is applicable to toxicology, pharmacology, fertility, animal husbandry, and the design of micro devices for sperm selection and sorting in IVF. This paper is tailored toward research rather than clinical application. Typically, research video data is better quality than that captured by typical CASA systems. In addition, the sperm in both datasets used in this paper are suspended in fluid of higher viscosity than IVF fluid, which is a mixture of saline and water. Using a more viscous fluid slows the sperm progression, allowing researchers to easily analyze flagellar beating patterns. Our approach affords researchers the opportunity to visualize 17 explicit and 3 implicit parameters for each sperm simultaneously in a static scene by reintroducing position, orientation and time into the visual analysis. We therefore use our glyphs in two ways, firstly as a summary glyphs (Section 7.2) and secondly to analyze the sperm tracks of specific sperm cells (Section 7.3).

### 7.1 Data Sources

Motility data for different mammals was collected from a number of sources in the biology literature [31], [54], [42], [51], [62], [18], [1]. Sources such as Cummins *et al.* [12] provides a comprehensive list of average mammalian sperm motility measurements. In addition to this the domain specialists provided us with two videos to analyze. The first video of a single sperm cell from a normal research donor was captured with a Olympus BX-50 microscope, positive phase contrast and Hamamatsu C9300 CCD Camera at a framerate 293.4Hz, pixel size  $7.4\mu\text{m}$  at 20x magnification. The medium is Earle's balanced salt solution with sodium lactate, sodium pyruvate, without phenol red and viscosity increased with Sigma M7140 Methylcellulose 2%, nominal viscosity 15 cPoise or 0.015Pa.s with no stage heater (ambient temperature). The sperm had migrated into a  $400\mu\text{m}$  depth, 4mm width capillary Kremer test assay. The sperm in the image was at approximately 2cm migration distance. The second video was filmed under similar conditions except at a lower framerate 50Hz. The swimming medium is also different, human tubal fluid, an IVF medium was used instead with viscosity increased with Sigma M0262 Methylcellulose 2% (nominal viscosity 400cPoise or 0.4 Pa.s). The sperm had migrated 1cm into a  $400\mu\text{m}$  depth, 4mm width capillary Kremer test assay.

One question biologists and clinicians are eager to answer about sperm is, “what characterize normal motility?”, i.e., how do the good sperm that make it through the cervix swim? In particular, what do their flagella do kinematically and mechanically? Answering this question would provide the baseline for assessing the effect of drugs, toxic effects, temperature, pH etc. Answering a general question like this beyond the scope of this paper but we are able to use glyphs to answer a number of more specific questions the biologist have about sperm function. The biologist chose three sperm cells exhibiting swimming patterns of interest. One straight swimming cell in low viscosity fluid and two more cells

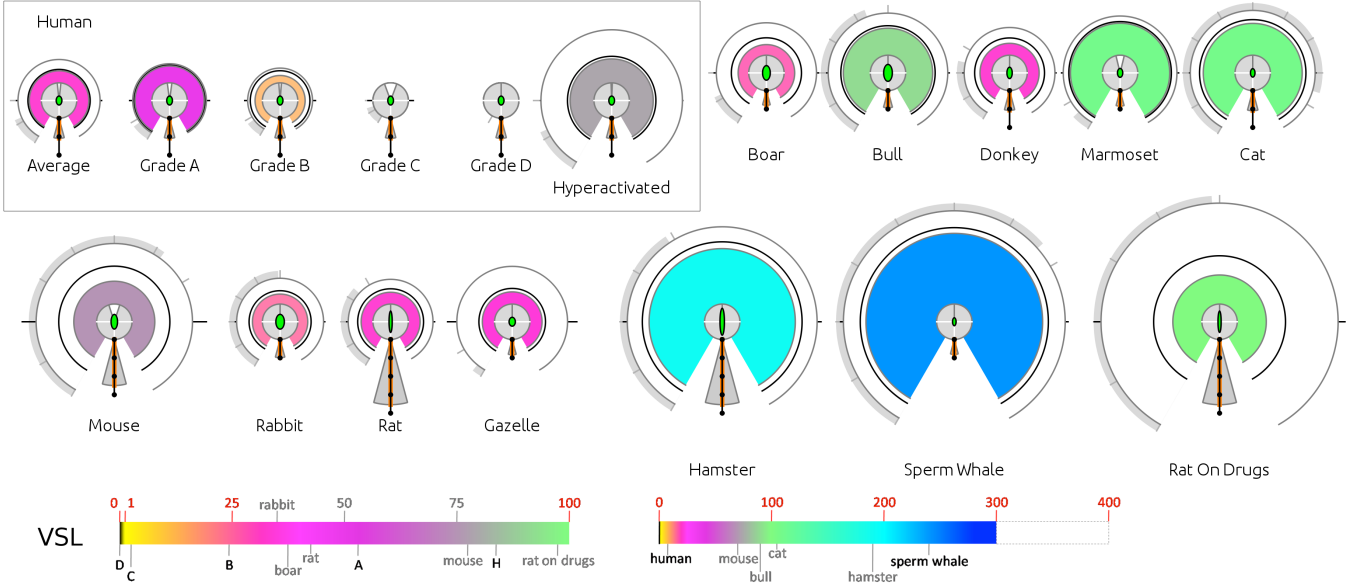


Fig. 7: The average sperm glyphs for multiple species with VSL colormap. Human sperm glyphs are shown with CASA system grading. CASA measures for other species were gathered from the research literature.

in high viscosity fluid, a straight swimmer and a circular swimmer. The circular swimming pattern often indicates sperm dysfunction. We use glyphs to answer the following:

- 1) Is analysis in high viscosity better than in low viscosity?
- 2) Which kinematic measures indicate dysfunction?
- 3) Which mechanical measures indicate dysfunction?
- 4) What ranges of values characterize normal function?

The last question will be impossible to answer with such a small sperm population but it is a current grand challenge for biomathematicians.

## 7.2 Summary Glyphs

One application of semen analysis is in inter-species comparison of cell function. These comparisons are used in an attempt to define average values and standard ranges of parameters for sperm cells as discussed by Holt *et al.* [30]. Ultimately they are used for toxicology, andrology and designing micro devices for cell selection. Fig. 7 shows a set of summary glyphs encoding a number of kinematic measures for cells of different species. For the flagellum only arclength is encoded by the glyphs as the other parameters were not available in the literature. To indicate this the uncertainty of the flagellum is set to 0.75. Fig. 7 provides insight into the differences in sperm behavior across species. In addition, it shows the flexibility of our glyph design. The grading system for humans sperm cells from the WHO manual [68] is as follows: *Grade A*: rapidly progressive motility; *Grade B*: slow or sluggish progressive motility; *Grade C*: non-progressive motility. *Grade D*: immotility. *Grade H* are hyperactivated sperm, exhibiting asymmetric and irregular beat patterns and high velocities associated with fertilization and penetration of the oocyte. In conjunction with the colormap it is easy to compare velocities of sperm. For example, the “*Rat On Drugs*” dosed with EGEE (ethylene glycol monoethyl ether), a toxin that is known to affect sperm motility, has high VCL and medium VSL

indicating less progressive erratic swimming; while the sperm whale shows that fastest VSL with slower VCL than the dosed rat indicating more progressive swimming. The sperm whale in comparison shows a lower VSL to VCL ratio than the dosed rat, despite having lower velocity; this indicates more progressive swimming.

Fig. 8 shows the summary glyphs for three cells as discussed in Section 7.1. The sperm cell in low viscosity, Fig. 8(a), is a straight swimmer. However, it shows a high VCL in comparison to VAP and VSL, indicating an erratic swimming pattern. This could be misinterpreted as non-progressive swimming. The two sperm cells in high viscosity show much more progressive swimming patterns by exclusively examining the velocities. However, only Fig. 8(b) is progressively swimming, Fig. 8(c) is actually swimming in circles and is dysfunctional. A pattern that would not appear so clearly in low viscosity, indicating that for analysis, high viscosity is better. It is clear that in high viscosity, the kinematic parameters that indicate circular swimming are high ALH, low BCF, large difference between VCL and VSL indicate a circular swimmer. For mechanical parameters, asymmetric beating and low torque indicate circular swimming. While two cells are not enough to make any substantial claims, it is clear the glyphs give direct insight into the data and save the biologist time in analysis.

## 7.3 Glyph Tracks

Summary glyphs are useful but without viewing the glyph tracks it is more difficult to identify dysfunctional cells. We address the same questions as in Section 7.1 in terms of glyph tracks in Fig. 9. Here one glyph is rendered for each second of the video as discussed in previous sections. The erratic swimming pattern of the low viscosity swimmer in Fig. 9(a) is indicated by the shape of the path and the difference in VCL to VSL in comparison to the high viscosity cells. This reiterates the fact that the swimming patterns of the high

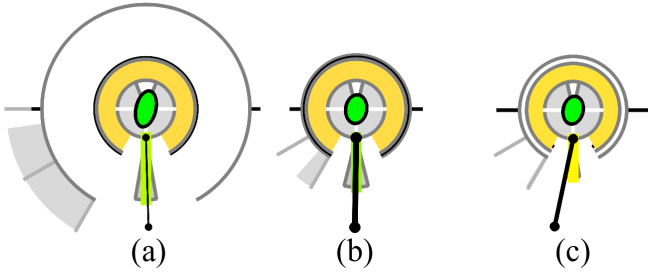


Fig. 8: Summary glyphs comparing low viscosity swimmers in (a) with high viscosity swimmers in (b) and (c). These glyphs allow us to immediately answer a number of questions asked by the biomathematicians in Section 7.1

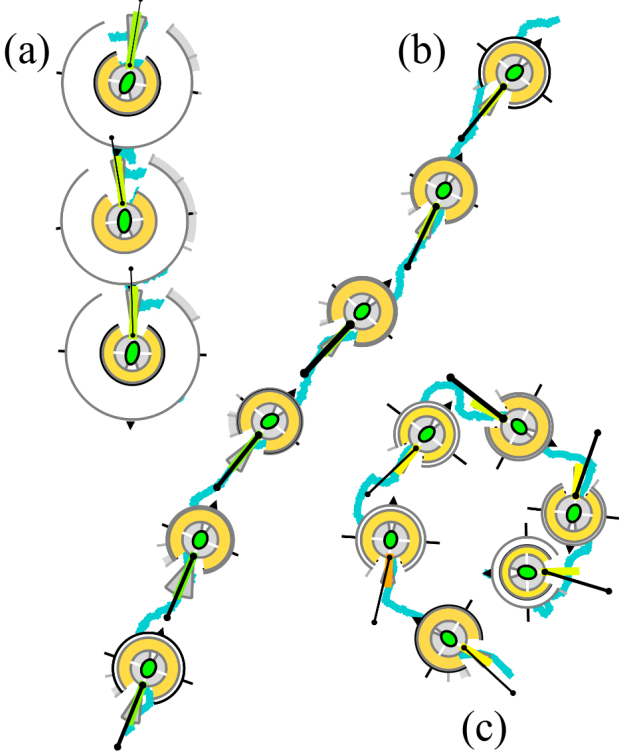


Fig. 9: Glyph tracks comparing low viscosity swimmers in (a) with high viscosity swimmers in (b) and (c). Glyph track view is useful for discovering swimming patterns and comparing parameters of each cell as they progress.

viscosity cells are clearer in these visualizations. The circular swimming pattern of the cell in Fig. 9(c) is immediately obvious. The swimmer in Fig. 9(b) shows periodic changes in parameter values across the track. While the swimmer in Fig. 9(c) shows less consistent periodicity. Again for the kinematic parameters, the circular swimmer shows high ALH, low BCF and aperiodic fluctuation in VCL and VSL. For the mechanical parameters, the flagellum is always asymmetric to the left, where in comparison the straight swimmer which is nearly always centered. The torque fluctuates aperiodically in the circular swimmer over a greater range where as for the straight swimmer the fluctuations are periodic and over a smaller range. It may be the torque estimates are unreliable as the uncertainty in flagellum tracking is high.

Here we note that we are more likely to rely on the

kinematic measures of the cells in these visualizations. The heads of the cells are consistently tracked with 100% certainty. While the certainty of the flagellum tracking is lower. For the circular swimmer this tracking is the worst. Including certainty measures for the tracking allows us to be more objective about our conclusions for this data. Additionally, we know the average length of a human sperm cell is  $50\mu m$  and is encoded into the pendulum. The arc length of the flagella of these cells consistently falls short of that average for two reasons. Firstly because of errors in tracking the flagellum. Secondly because the arc length is a projection of the flagellum into 2D. The combination of uncertainty measure and average length ruler allows to rationalize about the tracking and how much 3D movement is occurring in the flagellum beating pattern.

## 8 IMPLEMENTATION

In implementing this system an extreme programming approach was used, under the guidance of the biomathematicians. To allow rapid prototyping of the system we used Python as a trade off for speed. Typically biomathematicians are limited to sperm populations of less than 20 cells. Our system easily handles 11 cells at interactive frame rates. The bottleneck in the system is the computation of the integrals of the motion measures, which are computed once for each cell. Semi-automated computer vision techniques are used to preprocess the video and extract the geometry of the cells to do the motion analysis. The performance of this system could be significantly improved upon porting to C++.

The glyphs and the interface are rendered using PyQt4 with OpenGL optimization. Glyphs are rendered using vector graphics and so the user can easily scale the glyph scene. In addition to this the interface mimics a real sample slide by allowing the user to grab and pan it around in the scene. A number of implementation issues arose while developing this system such as overlap and scaling. The layout of the glyphs to avoid overlap and scaling can be seen in Fig. 11. An interface was provided for scaling the glyphs by zooming the scene or by tweaking display parameters related to the drawing routines for the glyphs. This provided enough flexibility for the user to compensate for these issues.

## 9 EVALUATION BY DOMAIN EXPERTS

This work was conducted over a 12 month period in close collaboration with three domain experts who are co-authors of this paper and in areas of cell biology and biomathematics. The project was initially motivated by the difficulties in observing and measuring motion characteristics of sperms captured on video using conventional image analysis techniques, and in relating the video data to mathematical models built by biomathematicians. As we were fully aware of the fact that any attempt in devising an automated as well as practical solution using computer vision would be a long-term challenge, we formulated a video visualization solution to assist domain experts in observing data more efficiently. During a consultation meeting after the idea of glyph-based visualization was first formulated, the domain experts suggested a number of avenues for potential uses of such visualization. These include:

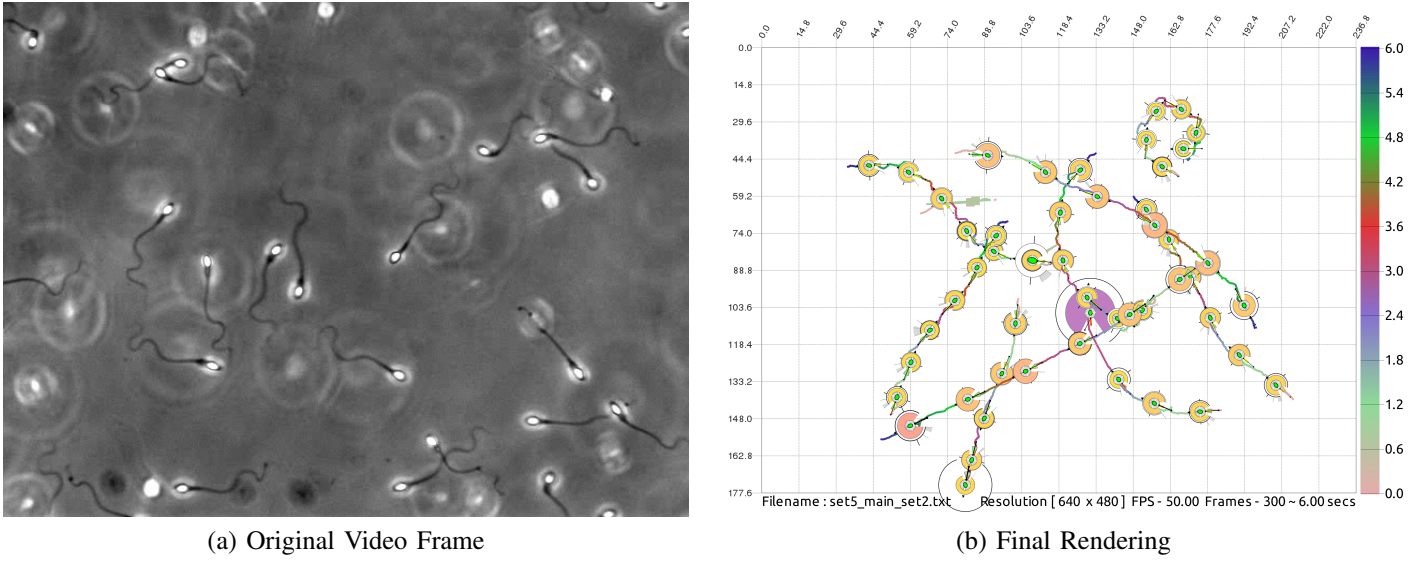


Fig. 10: Final rendering of 11 sperm cells in high viscosity fluid. A colormap encoding time is provided.

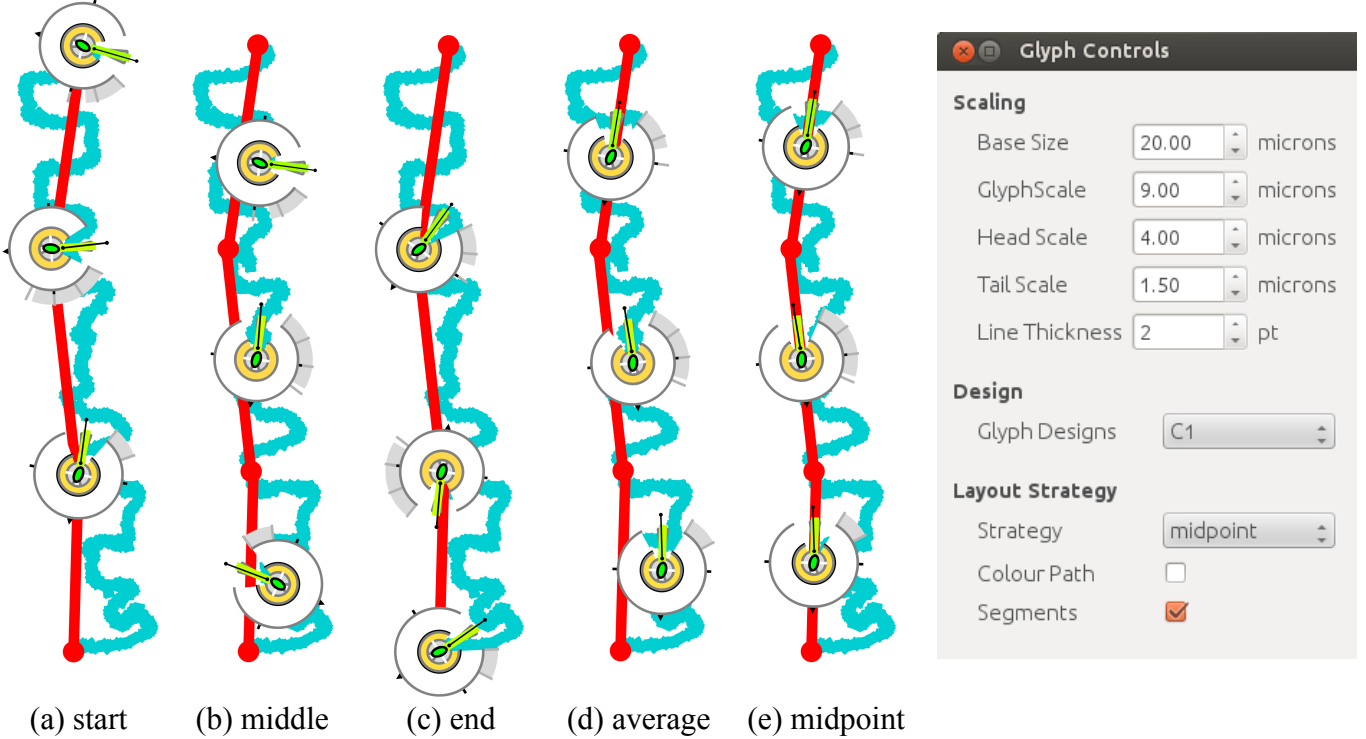


Fig. 11: Possible layouts for glyphs. The midpoint layout gives the most consistent layout. All glyph related parameters and settings can be tweaked in the application.

(a) alleviating the need for watching videos repeatedly, (b) summarizing multiple motion characteristics of sperms under investigation, (c) helping scientists comparing the motions of different cells, and (d) helping analysts in clinical semen analysis.

The evaluation of the usability of glyph-based visualization took several forms. In addition to close interaction with the three domain experts in the team, we interviewed domain experts in formally organized evaluation meetings. Furthermore, the first author was provided with a placement in the Institute of Reproductive Sciences in Oxford to gain

firstrand experience of sperm counting and semen analysis. This facilitated better understanding of the clinical procedures in practice and further interaction with the domain experts. These different forms of evaluation collectively confirmed the above-mentioned potentials in (a), (b) and (c). However, there was no evidence to support the potential in (d). We briefly described the discussions in the formally organized meetings after the visualization system was implemented.

**Meetings with Clinical Analysts.** In a half-day meeting, we sought advice and feedback from two domain experts at the Institute of Reproductive Sciences in Oxford. After

we presented our work, the discussion quickly shifted to the existing systems for semen analysis. We were informed that the current clinical practice focuses mainly on sperm counting. While computerized systems can automatically return meaningful numbers of sperm concentration, clinicians are fully aware of the fact that they are not accurate, especially when samples contain blood cells, bacteria, debris and other artifacts. Manual counting is a routine operation for embryologists in the Institute. An embryologist processes approximately 20 samples per day. There is an overwhelming demand for more accurate and cost-effective counting system. We realized that the domain experts mistook the visualization system as a computer vision system. We explained that the visualization is designed to supplement and complement the automatic vision system. Once the discussion was re-focused back to the use of visualization in semen analysis, the domain experts immediately suggested that it would be very useful to researchers. We therefore concluded that the visualization is not ready to support clinical semen analysis.

On the other hand, the two domain experts noted that glyph-based visualization would be useful for validating measurements obtained using automatic systems, and could also be used as a record for manual evaluation processes. They particularly liked our approach for considering both head and flagellum, and suggested the inaccuracy in many existing systems may result from counting the head only. The fact that the visualization can allow scientists and researchers to observe many measurements at the same time will be a big bonus. This indicated a potential for using visualization to help domain experts to make use of more measurements.

We explicitly sought advice from the domain experts as a means for improving the visualization. The domain experts pointed out that when two trajectories intersect with each other, it was difficult to ascertain whether there was a collision. The team took the problem of trajectory intersection back, and examined a number of design options, including the two suggestions by clinicians: 3D and opacity-based depth cue. Finally, we converged to a solution that uses a temporal colormap for displaying the trajectories.

**Meetings with Cell Biologists.** We organized a half-day consultation meeting with five domain experts (including cell biologists and biomathematicians) in Experimental Medicine at the University of Birmingham. This was followed by continuing interaction over six months for various software refinements. All domain experts appreciated that the visualization method developed in this project can alleviate the need for watching videos repeatedly. They also appreciated most aspects of our visual design, and agreed that it conveyed more information than any standard techniques. The experts were enthusiastic about the glyphs and regarded them as useful and metaphorically meaningful. In terms of using three circular arcs to represent VSL, VCL and VAP, the domain experts found that they are rather effective in comparison with any alternatives such as straight lines or color mappings. They considered the possibility of confusing with area mapping was not really an issue as professionals could learn to interpret new visual representations quickly. There were also discussions among the domain experts over which parameters should be

encoded and with what priority. The meeting concluded that it was better to maintain the generality of the current design.

Among all of the visualizations we presented, the domain experts found the aggregated glyphs, such as those in Fig. 7 the most informative. Although experts agreed that video summarization such as Fig. 10 encapsulated a substantial amount of information in a video, and could be used as a reminder as to what was in the video (i.e., external memorization), they found it cognitively more demanding to interpret than glyphs on a single track (e.g., Fig. 9). As there were many glyphs in a summary visualization, some domain experts wondered if it was possible for important changes to be emphasized visually. Although no evident example was found to support such a worry, the anxiety about a new technique was understandable, as was the instinct to revert to quantitative data (i.e., individual time series). This suggests that although glyph-based visualization is a novel technique, it cannot totally replace conventional techniques such as time series plots. Meanwhile, all experts agreed that visualizing several time series plots for each sperm would not scale up to many sperms captured on a video. The domain experts made a few suggestions of minor refinement of the visual designs, which were incorporated into the results presented in this paper. The experts also outlined some challenges in automatic detection and summarization of behavior changes of sperms, and clustering of similar sperms. These are beyond the scope of this paper.

## 10 CONCLUSIONS

We have developed a novel glyph-based video summarization for supporting semen analysis in a research settings. We made use of segmented sperm heads and flagella to compute a large set of motion characteristics. In consultation with domain experts, we addressed the demanding needs for encoding 20 dimensions by making use a compact glyph design. The glyph-based visualization enables users to observe various complex motion patterns that may be related to different measurements in a combinatory manner, serving as a summary of temporal activities. Hence, it reduces the need for scientists to watch videos repeatedly and reveals patterns and changes in sperm motility that were not previously observed using standard analysis techniques. We evaluated our work by consulting cell biologists, biomathematicians and clinical analysts. We took their advice and made improvement to our system. For future work, we will examine means for improving measurement accuracy in processing clinical videos by making use of advanced visual analytics techniques.

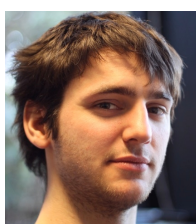
## ACKNOWLEDGMENTS

The authors wish to thank Akanksha Mishra and Celine Jones from the Institute of Life Sciences Oxford for the invaluable advice and feedback during the design process. We are also grateful to Drs David Foo and Hermes Gadêlha for discussions at Centre for Human Reproductive Science, Birmingham Women's NHS Foundation Trust. Imaging data were captured as part of DJS's Fellowship (Medical Research Council grant G0600178). This publication is based on work supported by Award No. KUK-C1-013-04, made by King Abdullah University of Science and Technology (KAUST).

## REFERENCES

- [1] T. Abaigar, W. V. Holt, R. A. P. Harrison, and G. del Barrio. Sperm subpopulations in boar (*sus scrofa*) and gazelle (*gazella dama mhorr*) semen as revealed by pattern analysis of computer-assisted motility assessments. *Biology of Reproduction*, 60(1):32–41, January 1999.
- [2] R. P. Amann and D. F. Katz. Reflections on CASA after 25 years. *Journal Of Andrology*, 25(3):317–325, 2004.
- [3] S. A. Baba and Y. Mogami. An approach to digital image analysis of bending shapes of eukaryotic flagella and cilia. *Cell Motility*, 5(6):475–489, 1985.
- [4] J. Bertin. *Semiology of graphics: diagrams, networks, maps*. University of Wisconsin Press, Madison, WI, 1983.
- [5] R. Borgo, A. Abdul-Rahman, F. Mohamed, P. W. Grant, I. Reppa, L. Floridi, and M. Chen. An empirical study on using visual embellishments in visualization. *IEEE Transactions on Visualization and Computer Graphics*, 18(12):2759–2768, 2012.
- [6] R. Borgo, M. Chen, B. Daubney, E. Grundy, H. Jänicke, G. Heidemann, B. Höferlin, M. Höferlin, D. Weiskopf, and X. Xie. State of the art report on video-based graphics and video visualization. *Computer Graphics Forum*, 31(8):2450–2477, 2012.
- [7] R. P. Botchen, S. Bachthaler, F. Schick, M. Chen, G. Mori, D. Weiskopf, and T. Ertl. Action-based multifield video visualization. *IEEE Transactions on Visualization and Computer Graphics*, 14(4):885–899, July 2008.
- [8] B. Burns, B. E. Shepp, D. McDonough, and W. Wiener-Ehrlich. The relation between stimulus analyzability and perceived dimensional structure. *Psychology of Learning and Motivation*, 12:77–115, 1978.
- [9] M. Chen, R. Botchen, R. Hashim, D. Weiskopf, T. Ertl, and I. Thornton. Visual signatures in video visualization. *IEEE Transactions on Visualization and Computer Graphics*, 12(5):1093–1100, 2006.
- [10] C. D. Correa and K.-L. Ma. Dynamic video narratives. *ACM Transactions on Graphics*, 29(3):88, 2010.
- [11] R. A. Crawfis and M. J. Allison. A scientific visualization synthesizer. In *In Proceedings of IEEE Visualization, VIS '91*, pages 262–267, Los Alamitos, CA, USA, 1991. IEEE Computer Society Press.
- [12] J. M. Cummins and P. F. Woodall. On mammalian sperm dimensions. *Journal of Reproductive Fertility*, 75(1):153–175, September 1985.
- [13] G. Daniel and M. Chen. Video visualization. In *In Proceedings of IEEE Visualization*, pages 409–416, 2003.
- [14] R. O. Davis and D. F. Katz. Computer-aided sperm analysis (CASA): image digitization and processing. *Biomaterials Artificial Cells And Artificial Organs*, 17(1):93–116, 1989.
- [15] W. C. de Leeuw and J. J. van Wijk. A probe for local flow field visualization. In *In Proceedings of IEEE Visualization, VIS '93*, pages 39–45, Washington, DC, USA, 1993. IEEE Computer Society.
- [16] P. Dollár, V. Rabaud, G. Cottrell, and S. Belongie. Behavior recognition via sparse spatio-temporal features. In *VS-PETS*, pages 65–72, 2005.
- [17] P. Dragicevic, G. Ramos, J. Biblioowicz, D. Nowrouzezahrai, R. Balakrishnan, and K. Singh. Video browsing by direct manipulation. In *In Proceedings of ACM CHI*, pages 237–246, 2008.
- [18] E. Flores, E. Taberner, M. M. Rivera, A. Peña, T. Rigau, J. Miró, and J. Rodríguez-Gil. Effects of freezing/thawing on motile sperm subpopulations of boar and donkey ejaculates. *Theriogenology*, 70(6):936–945, October 2008.
- [19] R. Fuchs and H. Hauser. Visualization of multi-variate scientific data. *Computer Graphics Forum*, 28(6):1670–1690, 2009.
- [20] E. A. Gaffney, H. Gadélha, D. J. Smith, J. R. Blake, and J. C. K. Brown. Mammalian sperm motility: Observation and theory. *Annual Review of Fluid Mechanics*, 43(1):501–528, 2011.
- [21] W. Gander, G. H. Golub, and R. Strelbel. Least-squares fitting of circles and ellipses. *BIT*, (34):558–578, 1994.
- [22] W. R. Garner. Interaction of stimulus dimensions in concept and choice processes. *Cognitive Psychology*, (8):98–123, 1976.
- [23] A. Girgensohn, D. Kimber, J. Vaughan, T. Yang, F. Shipman, T. Turner, E. Rieffel, L. Wilcox, F. Chen, and T. Dunnigan. Dots: support for effective video surveillance. In *In Proceedings of 15th International Conference on Multimedia, MULTIMEDIA '07*, pages 423–432, New York, NY, USA, 2007. ACM.
- [24] D. B. Goldman, B. Curless, S. M. Seitz, and D. Salesin. Schematic storyboarding for video visualization and editing. *ACM Transactions on Graphics (In Proceedings of SIGGRAPH)*, 25(3), July 2006.
- [25] J. Gray and G. J. Hancock. The propulsion of sea-urchin spermatozoa. *J Exp Biol*, 32(4):802–814, December 1955.
- [26] S. Handel and S. Imai. The free classification of analyzable and unanalyzable stimuli. *Perception and Psychophysics*, 12:108–116, 1972.
- [27] A. Hinting, F. Schoonjan, and F. Comhaire. Validation of a single-step procedure for the objective assessment of sperm motility characteristics. *International Journal of Andrology*, 11(4):277–287, 1988.
- [28] M. Hlawitschka, G. Scheuermann, and B. Hamann. Interactive glyph placement for tensor fields. In *In Proceedings of 3rd International Symposium on Visual Computing*, 2007.
- [29] M. Höferlin, E. Grundy, R. Borgo, D. Weiskopf, M. Chen, I. W. Griffiths, and W. Griffiths. Video visualization for snooker skill training. *Computer Graphics Forum*, 29(3):1053–1062, 2010.
- [30] W. V. Holt, J. O'Brien, and T. Abaigar. Applications and interpretation of computer-assisted sperm analyses and sperm sorting methods in assisted breeding and comparative research. *Reproduction, Fertility and Development*, 19(6):709–718, 2007.
- [31] M. Horimoto, Y. Isobe, Y. Isogai, and M. Tachibana. Rat epididymal sperm motion changes induced by ethylene glycol monoethyl ether, sulfasalazine, and 2,5-hexandione. *Reproductive Toxicology*, 14(1):55–63, 2000.
- [32] E. W. Jecht and J. J. Russo. A system for the quantitative analysis of human sperm motility. *Andrologia*, 5(3):215–221, 1973.
- [33] M. Kaneto, S. Kanamori, A. Hishikawa, and K. Kishi. Epididymal sperm motion as a parameter of male reproductive toxicity: sperm motion, fertility, and histopathology in ethinylestradiol-treated rats. *Reproductive Toxicology*, 13(4):279–289, 1999.
- [34] H. Kang, X. Chen, Y. Matsushita, and X. Tang. Space-time video montage. In *In Proceedings of IEEE Computer Vision and Pattern Recognition*, volume 2, 2006.
- [35] D. F. Katz and R. O. Davis. Automatic analysis of human sperm motion. *Journal of Andrology*, 8(3):170–181, 1987.
- [36] D. F. Katz, R. O. Davis, B. A. Delandmeter, and J. W. Overstreet. Real-time analysis of sperm motion using automatic video image digitization. *Computer Methods and Programs in Biomedicine*, 21(3):173–182, 1985.
- [37] D. E. Kime, M. Ebrahimi, K. Nysten, I. Roelants, E. Rurangwa, H. D. M. Moore, and F. Ollevier. Use of computer assisted sperm analysis (CASA) for monitoring the effects of pollution on sperm quality of fish: application to the effects of heavy metals. *Aquatic Toxicology*, 36(3–4):223–237, 1996.
- [38] G. Kindlmann and C.-F. Westin. Diffusion tensor visualization with glyph packing. *IEEE Transactions on Visualization and Computer Graphics*, 12(5):1329–1335, September–October 2006.
- [39] R. M. Kirby, H. Marmanis, and D. H. Laidlaw. Visualizing multivalued data from 2d incompressible flows using concepts from painting. In *In Proceedings of IEEE Visualization, VIS '99*, pages 333–340, Los Alamitos, CA, USA, 1999. IEEE Computer Society Press.
- [40] D. H. Krantz and A. Tversky. Similarity of rectangles: an analysis of subjective dimensions. *Journal of Mathematical Psychology*, 12:4–34, 1975.
- [41] R. Laramee, H. Hauser, H. Doleisch, B. Vrolijk, F. Post, and D. Weiskopf. The state of the art in flow visualization: Dense and texture-based techniques. *Computer Graphics Forum*, 23(2):203–221, 2004.
- [42] R. Lavara and M. Baselga. Correlation between CASA and asma parameters in rabbit semen. *Reproduction*, 38(2):381–386, 2005.
- [43] P. Legg, D. Chung, M. Parry, M. Jones, R. Long, I. Griffiths, and M. Chen. Matchpad: Interactive glyph-based visualization for real-time sports performance analysis. *Computer Graphics Forum*, 31(3):1255–1264, 2012.
- [44] F. Li, A. Gupta, E. Sanocki, L. He, and Y. Rui. Browsing digital video. In *In Proceedings of ACM CHI*, pages 169–176, 2000.
- [45] J. Lighthill. Flagellar hydrodynamics: J. V. Neumann lecture. *SIAM Rev.*, (18):161–230, 1976.
- [46] E. Maguire, P. Rocca-Serra, S.-A. Sansone, J. Davies, and M. Chen. Taxonomy-based glyph design – with a case study on visualizing workflows of biological experiments. *IEEE Transactions on Visualization and Computer Graphics*, 18(12):2603–2612, 2012.
- [47] S. T. Mortimer. A critical review of the physiological importance and analysis of sperm movement in mammals. *Human Reproduction Update*, 3(5):403–439, September 1997.
- [48] S. T. Mortimer. CASA-practical aspects. *Journal of Andrology*, 21(4):515–524, 2000.
- [49] M. Nienhaus and J. Döllner. Depicting dynamics using principles of visual art and narrations. *IEEE Computer Graphics and Applications*, 25(3):40–51, 2005.
- [50] N. Patel and I. Sethi. Video shot detection and characterization for video databases. *Pattern Recognition*, 30:538–592, 1997.
- [51] C. Person, T. Lester, M. Person, and R. Rorie. Computer-assisted analysis of sperm parameters after selection of motile sperm by either

- percoll gradient, filtration, or swim-up procedures. *AAES Research Series 553*.
- [52] F. Post, B. Vrolijk, H. Hauser, R. Laramee, and H. Doleisch. The state of the art in flow visualisation: Feature extraction and tracking. *Computer Graphics Forum*, 22(4):775–792, 2003.
  - [53] R. Ramos, G. and Balakrishnan. Fluid interaction techniques for the control and annotation of digital video. In *In Proceedings of 16th ACM Symposium on User Interface Software and Technology*, pages 105–114, 2003.
  - [54] T. Robeck, S. Gearhart, K. Steinman, E. Katsumata, J. Loureiro, and J. O'Brien. In vitro sperm characterization and development of a sperm cryopreservation method using directional solidification in the killer whale (*orcinus orca*). *Theriogenology*, 76(2):267–279, 2011.
  - [55] T. Ropinski, S. Oeltze, and B. Preim. Survey of glyph-based visualization techniques for spatial multivariate medical data. *Computers & Graphics*, 2011.
  - [56] T. Ropinski and B. Preim. Taxonomy and usage guidelines for glyph-based medical visualization. In *In Proceedings of 19th Conference on Simulation and Visualization*, pages 121–138, 2008.
  - [57] T. Ropinski, M. Specht, J. Meyer-spradow, K. Hinrichs, and B. Preim. Surface glyphs for visualizing multimodal volume data. In *In Proceedings of 12th Workshop on Vision, Modeling, and Visualization*, pages 3–12, 2007.
  - [58] M. Rubinstein, A. Shamir, and S. Avidan. Improved seam carving for video retargeting. *ACM Transactions on Graphics (SIGGRAPH)*, 27(3):1–9, 2008.
  - [59] K. Schoeffmann and B. L. Video browsing using interactive navigation summaries. In *In Proceedings of International Workshop on Content-Based Multimedia Indexing*, volume 7, pages 243–248, 2009.
  - [60] R. N. Shepard. Attention and metric structure of the stimulus space. *Journal of Verbal Learning and Verbal Behavior*, (1):54–87, 1964.
  - [61] D. J. Smith, E. A. Gaffney, H. Gadéha, N. Kapur, and J. C. Kirkman-Brown. Bend propagation in the flagella of migrating human sperm, and its modulation by viscosity. *Cell Motility and the Cytoskeleton*, 66(4):220–236, 2009.
  - [62] C. Tretipskul, K. Buranaamnuay, S. Koonjaenak, P. Tumaruk, and M. Techkumphu. The use of computer-assisted sperm analysis for discriminating series of motility pattern of frozen-thawed boar semen. *Thai Journal of Veterinary Medicine*, 40(1):25–30, 2010.
  - [63] V. S. Truong B. Video abstraction: A systematic review and classification. *ACM Transactions on Multimedia Computing, Communications and Applications*, 3(1), 2007.
  - [64] M. Ward. Multivariate data glyphs: Principles and practice. In *Handbook of Data Visualization*, pages 179–198. 2008.
  - [65] M. O. Ward. A taxonomy of glyph placement strategies for multidimensional data visualization. *Information Visualization*, 1(3/4):194–210, December 2002.
  - [66] C. Ware. *Visual Thinking: for Design*. Morgan Kaufmann, 2008.
  - [67] P. C. Wong, H. Foote, D. L. Kao, R. Leung, and J. Thomas. Multivariate visualization with data fusion. *Information Visualization*, 1(3/4):182–193, December 2002.
  - [68] World Health Organization. *WHO laboratory manual for the Examination and processing of human semen*. World Health Organization, 5th edition, 2010. Department of Reproductive Health and Research.



**Brian Duffy** received a BSc in computer science from University College Dublin, Ireland in 2006. He received his PhD in visualization and computer graphics from the same institution in 2011. He is currently working for the Oxford Centre for Computational and Applied Mathematics at the University of Oxford. His research interests include scientific visualization with application to mathematical problems.

**Jeyan Thiyagalingam** received his PhD degree in computer science from Imperial College, London, in 2005. At present, he is a James Martin Fellow at the University of Oxford. His research interests include high performance computing, parallel algorithms, efficient algorithms for image and video processing, target tracking, estimation and data processing.



**Simon Walton** completed his PhD in 2007 at Swansea University, focusing on the deformation of discretely sampled object representations using GPUs. He now works as a research associate at the Oxford e-Research Centre, Oxford University. His recent interests are in Video Visualization techniques with a focus on perceptual challenges of combining many different layers of information in the same scene.



**David J. Smith** is in Applied Mathematics at the University of Birmingham. He received his PhD from the same institution in 2006 and subsequently undertook multidisciplinary training in the Schools of Medicine and Mathematics, funded by MRC and Wellcome Trust, specialising in the biofluidynamics of sperm and cilia. He was appointed Birmingham Science City Fellow and Lecturer in 2009.



**Anne Trefethen** is Chief Information Officer, Professor of Scientific Computing and Associate Director of the e-Research Centre at Oxford University. Her career has spanned both industry and academia, including ten years in the USA, where she worked for Thinking Machines Corp and at the Theory Centre, Cornell University. Before coming to Oxford, Anne was a Director of the UK e-Science Core Programme and was VP for Research and Development at NAG Ltd. Anne's work has focused on high-performance computing and data intensive science and particularly on algorithms and software systems.



**Jackson C. Kirkman-Brown** received his PhD in reproductive science from the University of Birmingham in 2000. He has extensive experience in the study of signalling in sperm for human fertility. He is currently the lead scientist for Assisted Conception (IVF) services. His research interests are on improving diagnosis and refining rational treatments for infertility, alongside developing research in all aspects of patient treatment and care through multi-disciplinary collaboration. Currently his team of cell biologists are working with industrial and academic partners across a wide range of disciplines, such as mathematics, computer science, optical engineering, rheology, fluid mechanics and chemistry, examining human sperm motility and modulation.



**Eamonn A. Gaffney** MA PhD (Cantab). University Lecturer, Centre for Mathematical Biology, Mathematical Institute, University of Oxford. Research interests: biological and biomedical applications of mathematics including flagellated swimming mechanics, biological aspects of reaction diffusion systems ranging from self-organisation models to oxygen transport in tissue and models of cell movement, signalling and interaction.



**Min Chen** received the PhD degree from University of Wales in 1991. He is currently a professor of scientific visualization at Oxford University and a fellow of Pembroke College. Before joining Oxford, he held research and faculty positions at Swansea University (i.e., research officer from 1987, lecturer from 1990, senior lecturer from 1998 and professor from 2001). His research interests include visualization, computer graphics and human-computer interaction. His services to the research community include papers co-chair of IEEE Visualization 2007 and 2008, co-chair of Volume Graphics 1999 and 2006, member of many program committees and several editorial boards, and co-director of Wales Research Institute of Visual Computing. He is a fellow of BCS, EG and LSW.